Research Square

Preprints are preliminary reports that have not undergone peer review.
They should not be considered conclusive, used to inform clinical practice,
or referenced by the media as validated information.

Domain-swapped multimerization of recombinant Anti-Rh(D) scFv expressed in E. coli: structural and functional insights

Saleha Hafeez
National University of Sciences and Technology
Muhammad Asghar
muhammad.asghar@biol.lu.se
Lund University

Research Article

Keywords: Recombinant proteins, membrane proteins, single-chain fragment variable, domain-swapping, glycine-serine linker, multimerization, protein purification, potentiator-enhanced hemagglutination

Posted Date: April 27th, 2026

DOI: https://doi.org/10.21203/rs.3.rs-9185272/v1

License: This work is licensed under a Creative Commons Attribution 4.0 International License.
Read Full License

Additional Declarations: No competing interests reported.

Abstract

Background

Single-chain fragment variable are promising recombinant antibody fragments for diagnostic and research applications due to their small size and ease of bacterial expression. This study investigated the formation, structural organization, and functional behavior of domain-swapped anti-Rh(D) scFv multimers formed with different lengths of glycine-serine linkers and expressed in *Escherichia coli* Lemo21(DE3).

Results

Two constructs were designed in VH-L-VL format using flexible glycine-serine linkers of lengths $(G_4S)_4$ and $(G_4S)_6$. Structural prediction was performed using computational modeling, followed by molecular docking and MMPBSA analysis to evaluate intramolecular binding cooperativity among multimeric domains. Structural analysis showed that longer linker length improved structural assembly and promoted correct VH-VL domain pairing, facilitating the formation of functional dimers and trimers. Recombinant proteins were expressed under fast (0 μM L-rhamnose) and slow (500 μM L-rhamnose) induction conditions and purified sequentially. Under slow induction, monomeric expression was favored and functional multimer formation increased, whereas fast induction led to higher total multimer formation but reduced functional efficiency. ELISA-based binding assays demonstrated comparable affinity between monomeric and multimeric species. The dimeric construct of anti-Rh(D)-6 scFv exhibited predominantly monovalent binding behavior, while M-trimers and T-trimers showed distinct functional characteristics, with the T-trimer displaying slightly enhanced avidity. Hemagglutination assays confirmed that both anti-Rh(D)-4 and anti-Rh(D)-6 scFv multimers did not induce red blood cell hemagglutination under standard conditions, although mixed-field hemagglutination was observed under potentiator-enhanced conditions in anti-Rh(D)-6 scFv.

Conclusion

These findings demonstrate that linker length and controlled induction conditions influence the structural and functional assembly of scFv multimers.

Introduction

Single-chain fragment variables (scFvs) are recombinant proteins consisting of the variable regions of an antibody's heavy (VH) and light (VL) chains, connected by a flexible peptide linker [1]. Unlike full-sized antibodies, scFvs are smaller and simpler to produce, particularly in bacterial systems [1], making them attractive for therapeutic and diagnostic applications [2]. The compact size of scFvs allows them to be

easily engineered, but reduced structure can lead to issues with stability and binding affinity, as they lack the interdomain disulfide bonds present in traditional antibodies [3, 4].

The structural properties of scFvs are strongly influenced by the design of the linker connecting the VH and VL domains. The standard format of an scFv features a VH and VL domain linked by a peptide chain that is typically longer than 12 amino acids, often composed of flexible glycine and serine residues [5, 6]. Both VH-L-VL and VL-L-VH formats are functional, and varying the length of the linker allows for the creation of higher-order multimeric structures such as dimers, trimers, and tetramers, which can either bind a single antigen (monovalent) or multiple antigens (multivalent) [2, 7, 8, 9]. Shorter linkers favor multimerization by restricting VH-VL flexibility, whereas longer linkers favor monomer formation by allowing proper folding of individual scFv units [10].

Producing scFvs in *Escherichia coli* presents challenges, particularly when expressed in the cytoplasm, as the reducing environment prevents the formation of essential disulfide bonds. This problem can be mitigated by producing scFvs in the periplasmic space, where the oxidative environment supports disulfide bond formation, or by using engineered strains of *E. coli* that enable cytoplasmic disulfide bond formation [11]. Additionally, higher-order scFv multimers often form during bacterial production, which can complicate studies focused on functional monomers. While non-functional multimers generally do not interfere with experiments, functional multimers can interfere with results [10, 12, 13].

In our previous research, multimers of anti-A scFv were obtained using a 15 amino acid glycine-serine (GS) linker in *E. coli* BL21(DE3). Only the bivalent dimers were studied alongside monomers, and they were found to be non-functional [14]. In this study, we aimed to determine whether extending the linker length would allow higher-order multimers of anti-Rh(D) scFvs to retain functionality. To test this, we increased the GS linker length to 20 and 30 amino acids and used computational modeling to predict the 3D structures of anti-Rh(D) scFv monomers and multimers. The genes encoding antigen-Rh(D) and anti-Rh(D) scFvs with different linker lengths were cloned into the pET-28a(+) vector via restriction digestion and ligation. Protein expression was carried out in *E. coli* Lemo21(DE3) strain. Purification of antigen-Rh(D) was first carried out via a two-step process: Ni-NTA affinity chromatography, followed by immunoaffinity. In contrast, the anti-Rh(D) scFvs were purified via a three-step process: His-tagged proteins were first purified via Ni-NTA chromatography, followed by protein purification from Native PAGE gels and finally, functional proteins were isolated. Following purification, the effects of fast and slow induction rates on multimer formation were studied. Binding parameters were then determined using ELISA. Finally, to assess whether the multimers could cause hemagglutination of RBCs due to multiple antigen binding sites, standard and potentiator-enhanced hemagglutination assays were performed and hemagglutination was observed microscopically.

Materials and methods

2.1 Chemicals and apparatus

All the software and web servers used in this study were as follows: I-TASSER web server, LZerD web server, PyMOL 3.1, ProtParam tool and GROMACS 2025.3.

All the chemicals, reagents and molecular products used in this research were of high quality and analytical grade. Following are the specific molecular biology products used: Bio Basic prestained mid-range (20–120 kDa) protein ladder, Thermo Fisher PageRuler prestained protein ladder (10–250 kDa), Thermo Fisher HisPur Ni^{2+}-NTA resin, Superdex 200 Increase agarose-based resin, Cloud-Clone (rabbit) anti-histidine and HRP-conjugated anti-rabbit (caprine) antibodies, SolarBio TMB staining kit, Qiagen HisSorb (Ni-NTA) plates and Thermo Fisher Pierce protein A/G coated plates.

Fresh screened O+ blood was provided by NUST ASAB Diagnostics Lab Islamabad.

2.2 Protein modeling

The amino acid sequences for the anti-Rh(D) heavy chain variable region (VH) and light chain variable region (VL) were retrieved from accession numbers AAC13447.1 and AAC13488.1, respectively [15]. Two different scFv constructs were designed with a flexible GS linker connecting the VH and VL domains in a VH-L-VL format. The first construct, anti-Rh(D)-4, utilized a $(G_4S)_4$ linker, while the second, anti-Rh(D)-6, incorporated a $(G_4S)_6$ linker. A C-terminal Tobacco Etch Virus (TEV) cleavage site and a 6X-Histidine tag were added for purification. Initial structural models of the resulting scFvs, in both their closed monomeric form and open chain configuration, were generated using the I-TASSER web server [16]. Subsequently, the open chain scFvs were subjected to protein-protein docking using the LZerD web server [17] to obtain the final $(scFv)_x$ multimeric models, as illustrated in Fig. 1. All the structures were analyzed using PyMOL version 3.1 [18].

The amino acid sequence of antigen-Rh(D) was obtained from accession number QYS16062.1 [19]. Similar to anti-Rh(D) scFvs, a C-terminal TEV cleavage site and a 6X His-tag were added.

2.3 Molecular docking, MD simulations and MMPBSA

Molecular docking was performed to evaluate the feasibility of simultaneous multivalent antigen engagement by multimeric anti-Rh(D) scFv constructs and to assess whether additional binding is limited by steric or structural constraints. Molecular docking was performed using the LZerD web server, and complexes were selected based on the structural feasibility and location of antigen binding interactions. The chosen complexes were then subjected to 200 ns molecular dynamics (MD) simulations under physiological conditions using GROMACS 2025.3 [20].

Binding free energies were calculated using Molecular Mechanics Poisson-Boltzmann Surface Area (MMPBSA) analysis on the final 50 ns of equilibrated MD simulations. To evaluate the intramolecular cooperative binding affinity, a stepwise approach was employed: multimeric constructs were first docked with a single antigen-Rh(D), followed by MD simulation and MMPBSA calculation. The resulting complex

was then sequentially docked with a second and then a third antigen (for trimer), each time followed by MD simulation and MMPBSA analysis.

2.4 Design and cloning of gene of interest into pET-28a(+) vector

Three recombinant gene constructs (anti-Rh(D)-4 scFv [$(G_4S)_4$], anti-Rh(D)-6 scFv [$(G_4S)_6$], and antigen-Rh(D)) were obtained from Twist Bioscience (USA). The scFv constructs were designed to include the OmpA signal peptide at the N-terminus, while the antigen-Rh(D) construct was synthesized without a signal sequence. All genes were flanked by NcoI and XhoI sites and directionally cloned into the pET-28a(+) expression vector via standard restriction-ligation (protocol in Supplementary Materials). The designs of recombinant gene constructs are given in Supplementary Figure S1. The recombinant pET-28a(+) plasmids were then transformed into the dedicated expression strain, *E. coli* Lemo21(DE3), for controlled protein expression studies.

2.5 Production and purification of transmembrane protein antigen-Rh(D)

Production of the transmembrane antigen-Rh(D) was carried out in *E. coli* Lemo21(DE3). One liter of LB medium supplemented with chloramphenicol (34 µg/mL) and kanamycin (25 µg/mL) was inoculated with 10 mL of an overnight culture and grown at 37°C with shaking at 200 rpm until the OD_{600} reached 0.6. To optimize the folding and membrane insertion of the transmembrane antigen-Rh(D), T7 lysozyme expression was modulated using 100 µM L-rhamnose. Protein expression was induced with 400 µM IPTG, and cultures were incubated overnight at 20°C.

Following induction, cells were harvested by centrifugation at 7,000 rpm for 30 min at 4°C and washed with resuspension buffer. Cell lysis was performed by probe sonication for 15 min at 80–90% amplitude using 10-s on/30-s off cycles. The crude lysate was centrifuged at 14,000 rpm for 1 h, and the resulting pellet was washed three times with 1 mL of resuspension buffer (50 mM Tris, 200 mM NaCl, pH 8.0). The transmembrane antigen-Rh(D) was solubilized by resuspending the pellet in 10 mL of resuspension buffer containing 1% Triton X-100, followed by incubation at room temperature for 1 h. After incubation, the sample was centrifuged for 1 h at room temperature, and the supernatant was collected for purification [21].

Purification was performed using nickel affinity Ni-NTA chromatography followed by immunoaffinity purification. For Ni-NTA chromatography, 10 mL of the solubilized sample was incubated overnight at 12°C with 300 µL of HisPur Ni-NTA resin pre-equilibrated in resuspension buffer (50 mM Tris, 200 mM NaCl, pH 8.0) containing 0.05% Triton X-100, with constant shaking. The resin was subsequently washed several times with the same resuspension buffer. Detergent exchange [21] was carried out by washing the resin with wash buffer (50 mM Tris, 200 mM NaCl, 20 mM imidazole, and 0.02% n-dodecyl-β-D-maltoside DDM, pH 8.0), thereby replacing Triton X-100 with DDM. The transmembrane antigen-Rh(D)

was then eluted using elution buffer (50 mM Tris, 154 mM NaCl, 250 mM imidazole, 0.02% DDM, pH 7.4). Imidazole was subsequently removed by desalting on a PD-10 column.

The functional antigen-Rh(D) was further purified using immobilized anti-Rh(D) IgG on a protein A/G-coated ELISA plate (an overview of the experiment is given in Supplementary Figure S2). For immobilization, 100 µL of anti-Rh(D) IgG (10 µg/mL in phosphate-buffered saline (PBS)) was added to each well and incubated at 4°C with constant shaking overnight. The following day, the supernatant was removed, and the wells were washed several times with phosphate-buffered saline with Tween 20 (PBST) (pH 7.4) followed by PBS wash. Approximately 100 µL of the Ni-NTA purified sample was added to each well and incubated at 37°C for 1 hour. After incubation, the supernatant was removed and the bound antigen-Rh(D) was eluted by adding tris-buffered saline (TBS) elution buffer (pH 9) containing 0.02% DDM. The final product was lyophilized and stored at − 70°C.

2.6 Production and purification of anti-Rh(D) scFvs variants

For large-scale production, both anti-Rh(D) scFv variants (anti-Rh(D)-4 and anti-Rh(D)-6) were expressed separately in *E. coli* Lemo21(DE3). An overnight culture (100 mL) was used to inoculate 5 L of LB medium supplemented with chloramphenicol (34 µg/mL) and kanamycin (25 µg/mL). The culture was grown at 37°C with shaking at 200 rpm until the optical density at OD_{600} reached 0.6. Protein expression was induced under slow induction conditions with 400 µM IPTG at 30°C in the presence of 500 µM L-rhamnose, and induction was carried out for 5 hours with continuous shaking at 200 rpm. Following induction, periplasmic proteins were extracted by resuspending the cell pellets in 5 mL of ice-cold TES buffer (50 mM Tris, 2 mM EDTA, 20% sucrose, pH 7.2) and incubating for 4 hours at 4°C with shaking. The crude extracts were then collected and clarified by filtration through a 0.45 µm syringe filter.

His-tagged proteins were purified from the crude lysate by Ni-NTA chromatography using HisPur Ni-NTA resin under native conditions. For batch purification, 150 µL of resin was added to the crude lysate and incubated at 18°C with constant shaking for 24 h. The next day, the resin was washed several times with 1 mL of resuspension buffer (50 mM Tris, 200 mM NaCl, pH 8.0) to remove unbound proteins. Weakly bound proteins were removed by sequential washing with wash buffer A (50 mM Tris, 200 mM NaCl, 20 mM imidazole, pH 8.0) followed by wash buffer B (50 mM Tris, 200 mM NaCl, 50 mM imidazole, pH 8.0). His-tagged proteins were eluted by incubating the resin with 150 µL of elution buffer (50 mM Tris, 154 mM NaCl, 250 mM imidazole, pH 7.4) for 30 min at room temperature.

The eluted protein was further resolved by Native PAGE to separate individual multimeric species. The Ni-NTA purified sample was loaded onto a 10% Native PAGE gel, and after electrophoresis, the gel was sectioned according to molecular weight ranges (20–35 kDa, 40–55 kDa, and 70–100 kDa) using a protein ladder as a reference. Each gel slice was transferred to a 2 mL microcentrifuge tube containing 0.5 mL of TBS buffer, crushed with a Teflon pestle, and incubated at 37°C with shaking for 24 h. The samples were centrifuged and resuspended every 3 h. This purification step was repeated until all the proteins in the sample were separated.

Functional monomeric anti-Rh(D) scFvs were then purified using ELISA plates coated with antigen-Rh(D) (Supplementary Figure S3). Purified antigen-Rh(D) was immobilized on HisSorb (Ni-NTA) ELISA plates, with each well coated with 20 µg of antigen in TBS for 1.5 hours at room temperature, followed by washing with TBS containing 0.01% DDM. Anti-Rh(D) scFv samples (100 µL) were added to the coated wells and incubated for 1 h to allow specific binding. Wells were then washed thoroughly with TBS buffer A (pH 7.4) to remove unbound protein. Bound scFvs were eluted with 25 µL of Glycine-HCl buffer B (50 mM Glycine, pH 3.5) and immediately neutralized with 100 µL of TBS buffer C (pH 8.5). The recovered material was analyzed via western blotting, lyophilized and stored at − 70°C. This process was repeated until no functional scFv could be detected.

To separate functional multimers with defined valencies, complexes of multimers and antigen-Rh(D) (without histidine tag) were assembled at stoichiometric ratios corresponding to the antigen binding capacity of each multimer (i.e., dimer:antigen at 1:2 and trimer:antigen at 1:3). Complex formation was carried out in detergent-containing resuspension buffer (50 mM Tris, 154 mM NaCl, pH 7.5) consisting of 0.02% DDM and incubated for 30 min at room temperature. Following incubation, samples were clarified by filtration through a 0.45 µm syringe filter. Size-exclusion chromatography (SEC) was then performed using a Superdex 200 Increase 10/300 GL column equilibrated with the same detergent-containing buffer. Chromatography was carried out on a Bio-Rad NGC chromatography system Quest 10 plus at a constant flow rate of 0.5 mL/min, with a maximum injection volume of 500 µL per run. Fractions were collected at 0.5 mL intervals. The multimer-antigen complexes in the collected fractions were then dissociated by adding 100 µL of Glycine-HCl buffer (50 mM Glycine, pH 3) and immediately neutralized with 200 µL of TBS buffer C (pH 8.5).

Ni-NTA chromatography was performed on the neutralized fractions as described above to recover the separated his-tagged multimers. The final products were analyzed via western blotting, lyophilized, and stored at − 70°C. The molecular weights observed in western blot analysis were compared with the theoretical molecular weights calculated using the ProtParam tool [22].

2.7 Quantification of functional monomers and multimers of anti-Rh(D) scFv variants

To assess the effect of fast versus slow induction on monomer and multimer formation, both anti-Rh(D) scFv variants were expressed as described above in section 2.6. Briefly, 5 mL of overnight culture was used to inoculate 0.5 L of LB medium, and protein expression was induced with 400 µM IPTG in the presence of two different concentrations of L-rhamnose (0 and 500 µM). Induction was carried out for a total of 5 hours, and samples were collected after induction. Functional monomers and multimers were purified as described in section 2.6 (functional monomers were separated using SEC followed by Ni-NTA purification, using the same procedure as for the other multimeric species). The concentrations of functional monomers and multimers were quantified using an A_{280} assay on a NanoDrop spectrophotometer, and the percentage of functional protein was calculated using the formulas mentioned in supplementary materials.

2.8 Evaluation of the binding parameters of monomeric and multimeric anti-Rh(D) scFvs via ELISA

To evaluate and compare the binding parameters, including the dissociation constant K_D and maximum binding capacity B_{max}, of monomeric and multimeric anti-Rh(D) scFv variants, an ELISA-based binding assay was performed in triplicate. An overview of the experiment is given in Supplementary Figure S4. Anti-His tag IgG antibodies (10 µg/ml) were immobilized on protein A/G-coated ELISA plates. Histidine-tagged antigen-Rh(D) was then added and immobilized on the plates at a concentration of 5 nM. Serial dilutions (0.2 nM to 100 µM) of monomeric and multimeric anti-Rh(D) scFvs were prepared and added to the antigen-coated wells. The plates were incubated for 30 min at 37°C with gentle shaking to allow the scFv-antigen interaction. Following the washing steps to remove unbound molecules, wells were incubated with anti-His tag primary antibodies and HRP-conjugated secondary antibodies, as described previously [14]. Absorbance was measured at 450 nm. K_D and B_{max} values were calculated by nonlinear regression analysis using a one-site specific binding model in GraphPad Prism version 9.5.1 [23].

2.9 Evaluation of multimer-mediated RBC hemagglutination by standard and potentiator-enhanced hemagglutination (PEH) assays

To evaluate the ability of the multimers to induce hemagglutination, both standard and potentiator-enhanced hemagglutination (PEH) assays were performed. For the standard hemagglutination assay, 50 µL of O+ RBCs were incubated with 200 µL of the multimer preparation (10 mg/mL) for 30 min at 37°C. In the PEH assay, ficin, low-ionic-strength saline (LISS), and polyethylene glycol (PEG) were employed to reduce the intercellular distance below the native ~ 18 nm zeta-potential barrier [24, 25 26]. Sialic acid-rich glycoproteins on the RBC surface were first enzymatically cleaved using ficin. Briefly, 50 µL of O+ RBCs were incubated with 0.1% ficin for 15 min at 37°C under gentle agitation. Following enzymatic treatment, the RBCs were washed three times with cold normal saline and resuspended in LISS (0.17 M NaCl, 0.15 M phosphate buffer, 0.3 M sodium glycine). PEG 4000 was then added to a final concentration of 10%, followed by an additional 30 min incubation at 37°C. Subsequently, 200 µL of the multimer preparation (10 mg/mL) was added to the treated RBC suspension and incubated for 30 min at 37°C with gentle shaking to allow binding to antigen-Rh(D) on the RBC surface. Hemagglutination was confirmed microscopically using the 3,3',5,5'-tetramethylbenzidine (TMB) staining method as described previously [27, 28]. Negative-control RBCs processed in parallel without multimer addition were used for comparison.

Results

3.1 Protein modeling

Unlike the monomer, multimeric forms $(scFv)_x$ of anti-Rh(D) scFvs are multivalent and can therefore bind multiple copies of the same antigen. Closed, functional monomeric forms are shown in Supplementary Figure S5. Structural models of dimeric and trimeric scFvs generated from the open chain forms of anti-Rh(D)-4 and anti-Rh(D)-6 scFvs are shown in Fig. 2.

Modeling of the open chain anti-Rh(D)-4 scFv produced two non-functional and one partially functional dimer $(scFv)_2$, and one non-functional, one partially functional, and one fully functional trimer $(scFv)_3$. In dimer-A4 (Fig. 2A), the VH domains of the two chains paired with each other, as did the VL domains, placing the CDRs incorrectly and rendering the dimer non-functional. In dimer-B4 (Fig. 2B), the VH domain of one chain paired with the VL domain of the second chain, again resulting in misoriented CDRs. Dimer-C4 (Fig. 2C) was partially functional and monovalent, with only one correctly formed VH-VL pair displaying properly oriented CDRs. Among the trimeric models, trimer-A4 (Fig. 2D) contained a single functional binding site, trimer-B4 (Fig. 2E) was fully functional with all three VH-VL pairs correctly aligned, and trimer-C4 (Fig. 2F) was non-functional with all VH-VL pairs incorrectly formed.

Similarly, modeling of the open chain anti-Rh(D)-6 scFv yielded multiple dimeric and trimeric assemblies. Two dimers were completely non-functional. In dimer-A6 (Fig. 2G), the VH domains paired with each other and the VL domains paired similarly. In dimer-B6 (Fig. 2H), VH-VL pairing occurred but the CDRs were oriented in opposite directions, resulting in a non-functional configuration. Dimer-C6 (Fig. 2I) was partially functional and monovalent, with one correctly paired VH-VL domain and properly oriented CDRs. Dimer-D6 (Fig. 2J) was fully functional, with correct VH-VL pairing and all CDRs properly oriented for antigen binding. Among the trimers, trimer-A6 (Fig. 2K) was completely non-functional, trimer-B6 (Fig. 2L) was monovalent with only a single correctly paired VH-VL domain, and trimer-C6 (Fig. 2M) was fully functional with all VH-VL pairs correctly aligned and their CDRs properly oriented. Figure 3 illustrates a comparison of the dimensions of the functional multimers formed by the open chains of anti-Rh(D)-4 and anti-Rh(D)-6 scFvs.

3.2 Molecular docking, MD simulations and MMPBSA

Molecular docking was conducted to assess whether multimeric anti-Rh(D) scFv constructs are structurally capable of engaging multiple antigen molecules simultaneously or whether structural constraints limit antigen binding site accessibility. As shown in Fig. 4, the monomeric forms of both anti-Rh(D)-4 (Fig. 4A) and anti-Rh(D)-6 (Fig. 4C) scFvs formed stable complexes with antigen-Rh(D), with antigen binding domains properly oriented toward the target. In the dimeric anti-Rh(D)-6 scFv construct (Fig. 4D), only one binding domain could be successfully docked. Structural analysis revealed that the second site was oriented inward and sterically occluded, preventing formation of an additional antigen complex. In contrast, the trimeric forms of anti-Rh(D)-4 (Fig. 4B) and anti-Rh(D)-6 (Fig. 4E) scFvs accommodated three antigen-Rh(D) molecules. All three binding domains in both trimers were outward-facing and accessible, allowing simultaneous antigen engagement without interdomain steric interference.

Binding free energies were calculated using MMPBSA from the final 50 ns of equilibrated trajectories (Table 1). The monomeric anti-Rh(D)-4 and anti-Rh(D)-6 scFv constructs exhibited binding free energies of − 48.8 kcal/mol and − 48.6 kcal/mol, respectively. The dimeric anti-Rh(D)-6 scFv construct showed a binding free energy of − 49.0 kcal/mol for the single accessible binding site. For the trimeric anti-Rh(D)-4 scFv construct, sequential binding free energies were − 48.7 kcal/mol (first), − 48.5 kcal/mol (second), and − 48.8 kcal/mol (third). For the trimeric anti-Rh(D)-6 scFv construct, binding free energies were − 48.9 kcal/mol (first), − 49.2 kcal/mol (second), and − 48.7 kcal/mol (third). The comparable binding free energies observed across sequential binding events indicate non-cooperative intramolecular binding affinity within the multimeric constructs.

Table 1
MMPBSA-calculated binding free energies (ΔG_{Bind}, kcal/mol) for monomeric and multimeric anti-Rh(D) scFv complexes with antigen-Rh(D).

ScFvs	Monomer	B-Dimer (bivalent dimer)		T-Trimer (trivalent trimer)		
		First binding	Second binding	First binding	Second binding	Third binding
Anti-Rh(D)-4	−48.8	-	-	−48.7	−48.5	−48.8
Anti-Rh(D)-6	−48.6	−49.0	-	−48.9	−49.2	−48.7

3.3 Purification of antigen-Rh(D) and anti-Rh(D) scFv variants

The transmembrane protein antigen-Rh(D) was purified using a two-step process, and all fractions were analyzed via western blotting. As shown in Fig. 5A, the supernatant (S) from the crude lysate did not show any detectable bands, whereas the pellet (P) exhibited a single band at ~ 45 kDa. A band of similar molecular weight was also observed in the R-Tx fraction (lane 7), indicating that antigen-Rh(D) was successfully solubilized into the supernatant prior to chromatographic purification.

The first purification step involved Ni-NTA affinity chromatography of His-tagged antigen-Rh(D). No antigen-Rh(D) band was detected in the wash fraction (W), whereas the elution fraction (E) displayed a distinct ~ 45 kDa band corresponding to purified antigen-Rh(D). The second purification step employed immobilized anti-Rh(D) IgG antibodies to isolate functional antigen-Rh(D). The final purified eluate (FPE) showed a clear ~ 45 kDa band, confirming the successful isolation of functional antigen-Rh(D).

The purification of anti-Rh(D) scFv variants was carried out using a sequential three-step process. In the first step, both anti-Rh(D)-4 and anti-Rh(D)-6 scFvs were purified as His-tagged proteins. Analysis of the elution fractions ANiE and BNiE revealed distinct bands at ~ 25 kDa, ~ 50 kDa, and ~ 75 kDa (Fig. 5B), corresponding to the monomeric, dimeric, and trimeric forms, respectively.

In the second step, the scFv multimers were separated via Native PAGE electrophoresis. Fractions AN-1 to AN-3 contained the trimeric (~ 75 kDa), dimeric (~ 50 kDa) and monomeric (~ 25 kDa) species of anti-Rh(D)-4 scFv, while fractions BN-1 to BN-3 contained the corresponding multimeric and monomeric forms of anti-Rh(D)-6 scFv.

The purification of functional monomers was performed using immobilized antigen-Rh(D). Analysis of fractions AF-1 and BF-1 confirmed the successful purification of functional anti-Rh(D)-4 and anti-Rh(D)-6 monomers (~ 25 kDa), respectively. Theoretical molecular weights of purified protein species are given in Supplementary Table S3.

To isolate multimeric species with defined valencies, multimer-antigen complexes were separated by SEC, and the collected fractions were analyzed following dissociation and Ni-NTA purification.

SEC profile of anti-Rh(D)-4 scFv dimers (Fig. 6A) revealed two distinct peaks with elution maxima at approximately 17.5 mL (peak 1) and 19 mL (peak 2). Peak 1 exhibited a higher OD signal than peak 2. Western blot analysis (Fig. 6E) of the recovered fractions (lanes 3 and 4) identified F1 (derived from peak 1) as the free antigen-Rh(D) (~ 45 kDa) and F2 (derived from peak 2) as the free dimer (~ 50 kDa). SEC profile of anti-Rh(D)-4 scFv trimers (Fig. 6B) revealed four peaks with elution maxima at approximately 10 mL (peak 1), 13 mL (peak 2), 16 mL (peak 3), and 17 mL (peak 4). Peak 2 showed the highest OD intensity, followed by peak 1. Western blot analysis confirmed F3 (from peak 1) as the trivalent trimer-antigen (T-trimer-antigen) (~ 210 kDa) and F4 (from peak 2) as the monovalent trimer-antigen (M-trimer-antigen) (~ 120 kDa) (theoretical molecular weights of complexes are given in Supplementary Table S4). Peaks 3 and 4 yielded bands at ~ 45 kDa (F5) and ~ 75 kDa (F6), which were consistent with those of the free antigen and free trimer, respectively.

Similarly, SEC profile of anti-Rh(D)-6 scFv dimers (Fig. 6C) revealed three peaks with elution maxima at approximately 14.5 mL (peak 1), 17.5 mL (peak 2), and 18.5 mL (peak 3). Peak 1 displayed the highest OD among the three peaks. Western blot analysis (Fig. 6E) (lane 9) identified F1 (derived from peak 1) as the dimer-antigen complex (~ 95 kDa). Later-eluting (lane 10 and 11) peaks corresponded to (F2) free antigen (~ 45 kDa) and (F3) free dimer (~ 50 kDa). SEC profile of anti-Rh(D)-6 scFv trimers (Fig. 6D) showed four peaks with elution maxima at approximately 10 mL (peak 1), 13 mL (peak 2), 16 mL (peak 3), and 17 mL (peak 4). Peak 1 showed the highest OD intensity, followed by peak 2, whereas peaks 3 and 4 exhibited lower signals. Western blot analysis (lanes 8–14) confirmed fraction F4 (derived from peak 1) as the T-trimer-antigen complex (~ 210 kDa) and F5 (derived from peak 2) as the M-trimer-antigen complex (~ 120 kDa). Peaks 3 and 4 contained bands at ~ 45 kDa and ~ 75 kDa, corresponding to the (F6) free antigen and (F7) free trimer, respectively.

Following Ni-NTA purification (Fig. 6E, lanes 17–21), EF1 and EF2 contained the T-trimer (~ 75 kDa) and M-trimer (~ 75 kDa) species of anti-Rh(D)-4 scFv, which were purified from peaks 1 and 2 (Fig. 6B), respectively. In contrast, EF3, EF4, and EF5 corresponded to anti-Rh(D)-6 scFv species: EF3 contained the T-trimer (~ 75 kDa) purified from peak 1 (Fig. 6D), EF4 contained the M-trimer (~ 75 kDa) purified from peak 2 (Fig. 6D), and EF5 contained the dimer (~ 50 kDa) purified from peak 1 (Fig. 6C).

3.4 Quantification of the formation of monomers and multimers of anti-Rh(D) scFv variants

To evaluate how induction rate affects multimer formation, anti-Rh(D)-4 and anti-Rh(D)-6 scFvs were expressed under fast and slow induction with 0 and 500 μM L-rhamnose.

The induction rate had a significant impact on the multimerization of anti-Rh(D)-4 and anti-Rh(D)-6 scFvs. Faster induction conditions (0 μM L-rhamnose) generally promoted the accumulation of dimers and trimers, whereas slower induction (500 μM) favored the monomeric state. For anti-Rh(D)-4 scFv (Table 2), slower induction (500 μM) resulted in trimers and dimers comprising 28.7% and 25.7%, respectively, with monomer as the dominant species at 45.6%. In contrast, fast induction (0 μM) increased multimer formation, with trimers and dimers reaching 37.8% and 40.2%, while monomer decreased to 17.8%.

Anti-Rh(D)-6 scFv exhibited a similar pattern. Under slow induction (500 μM), monomer remained the major species at 47.4%, with trimers and dimers at 31.2% and 18.5%, respectively. Faster induction (0 μM) shifted the distribution toward multimers, increasing trimers to 45.2% and dimers to 30.7%, while monomer decreased to 23.8%.

Table 2
Effect of induction rate on overall multimer formation of anti-Rh(D)-4 and anti-Rh(D)-6 scFvs.

ScFvs	L-Rhamnose (μM)	Trimer (%)	Dimer (%)	Monomer (%)
Anti-Rh(D)-4	500	28.7	25.7	45.6
	0	37.8	40.2	17.8
Anti-Rh(D)-6	500	31.2	18.5	47.4
	0	45.2	30.7	23.8

Functional multimer formation exhibited distinct patterns relative to total multimer distribution (Table 3). For anti-Rh(D)-4 scFv, trimer functionality increased under higher L-rhamnose concentration, with T-trimer functionality reaching 21.55% and M-trimer functionality 33.26% at 500 μM induction. Under fast induction conditions (0 μM L-rhamnose), T-trimer and M-trimer functionalities were 7.70% and 12.70%, respectively. Monomer functionality remained consistently higher across conditions, measuring 88.32% at 0 μM and 76.41% at 500 μM, resulting in overall functional activities of 24.31% and 50.55% under 0 μM and 500 μM induction, respectively.

In contrast, anti-Rh(D)-6 scFv demonstrated higher functional multimer assembly across all species. Under slow induction (500 μM L-rhamnose), functional levels were notably elevated, with T-trimer functionality at 65.70%, M-trimer at 20.32%, dimer at 81.71%, and monomer at 89.73%, yielding an overall functional activity of 86.98%. Fast induction conditions (0 μM L-rhamnose) resulted in comparatively

lower functional proportions, with T-trimer at 11.76%, M-trimer at 5.95%, dimer at 33.44%, and monomer at 64.33%, corresponding to an overall functional activity of 35.46%.

Table 3
Effect of induction rate on functional multimer formation of anti-Rh(D)-4 and anti-Rh(D)-6 scFvs.

ScFvs	L-Rhamnose (μM)	T-Trimer Functional (%)	M-Trimer Functional (%)	Dimer Functional (%)	Monomer Functional (%)	Overall Functional (%)
Anti-Rh(D)-4	500	21.55	33.26	0.00	76.41	50.55
	0	7.70	12.7	0.00	88.32	24.31
Anti-Rh(D)-6	500	65.70	20.32	81.71	89.73	86.98
	0	11.76	5.95	33.44	64.33	35.46

3.5 Comparison of the binding parameters of monomeric and multimeric anti-Rh(D) scFv variants

The binding affinity (dissociation constant K_D) and binding capacity (B_{max}) were determined to compare the binding parameters of monomeric and multimeric forms of both anti-Rh(D) scFv variants. As shown in Fig. 7A, the monomer of anti-Rh(D)-4 scFv exhibited a K_D of 0.332 μM and a B_{max} of 0.770. The M-trimer displayed very similar binding parameters, with a K_D of 0.328 μM and a B_{max} of 0.776, indicating no significant enhancement in binding affinity and suggesting a predominantly monovalent binding behavior. In contrast, the T-trimer showed a lower K_D of 0.247 μM and a reduced B_{max} of 0.694, consistent with increased apparent affinity and indicative of multivalent binding effects.

Similarly, for anti-Rh(D)-6 scFv (Fig. 7B), the monomer and dimer demonstrated comparable binding characteristics, with K_D values of 0.327 μM and 0.314 μM and B_{max} values of 0.716 and 0.723, respectively, supporting a monovalent mode of interaction. The M-trimer also showed similar affinity, with a K_D of 0.329 μM and a B_{max} of 0.707. In contrast, the T-trimer exhibited a markedly lower K_D of 0.232 μM accompanied by a decreased B_{max} of 0.663, suggesting enhanced binding avidity attributable to multivalent interactions.

3.6 Multimer-mediated RBC hemagglutination assessed by standard and potentiator-enhanced hemagglutination (PEH) assays

Standard and PEH assays were used to assess the ability of multimeric anti-Rh(D) scFvs to mediate hemagglutination of RBCs. The O+ RBCs readily hemagglutinated in the presence of anti-Rh(D) IgM antibodies (Fig. 8A). RBCs subjected to the PEH assay in the absence of anti-Rh(D)-4 scFvs remained non-hemagglutinated, indicating that the three-step potentiator-enhanced process alone did not promote

cell clumping (Fig. 8B). RBCs coated with the T-trimeric anti-Rh(D)-4 scFv did not hemagglutinate under standard conditions (Fig. 8C) and remained non-hemagglutinated after the PEH assay (Fig. 8D).

The O+ RBCs coated with dimers of anti-Rh(D)-6 scFv did not hemagglutinate under either standard conditions (Fig. 9A) or potentiator-enhanced conditions (Fig. 9B). In contrast, RBCs coated with the T-trimer of anti-Rh(D)-6 scFv did not hemagglutinate under standard hemagglutination conditions (Fig. 9C), but mixed-field hemagglutination was observed after the PEH assay (Fig. 9D).

Discussion

Single-chain fragment variables are attractive antibody fragments due to their small size and ease of bacterial production, but their tendency to form unwanted multimers can limit analyses of monomeric species. Here, we examined the structure and function of domain-swapped (scFv)₂ multimers formed during expression of anti-Rh(D) scFvs in *E. coli* Lemo21(DE3), with particular emphasis on the impact of GS linker extension on their structural organization and functional potential. Building on earlier observations that short linkers favor non-functional bivalent dimers and the formation of higher-order multimers, we assessed whether increased linker length supports the assembly of higher-order multimers while preserving antigen binding activity [10, 14].

Similar to IgG and IgM antibodies, scFv multimers (scFv)₂ are multivalent and can be engineered to be mono- or multispecific. These multimers can be generated either as tandem scFvs, in which multiple scFv units are linked within a single polypeptide, or through domain swapping between individual scFv monomers [9]. In this study, we used the conventional VH-L-VL scFv format to model multimeric assemblies of domain-swapped anti-Rh(D) scFvs.

Structural modeling (Fig. 2) highlighted the strong influence of linker length on domain pairing and the functional assembly of domain-swapped anti-Rh(D) scFv multimers. For both scFv variants, the modeled closed dimeric assemblies (Figs. 2A, 2B, 2G and 2H) were predominantly non-functional, whereas open chain dimers were observed only in a monovalent configuration containing a single correctly formed antigen binding site. Fully functional bivalent dimers were observed exclusively for the anti-Rh(D)-6 scFv variant incorporating the longer linker. A plausible explanation is that similar to previously reported [14] the short GS linker in anti-Rh(D)-4 scFv restricts domain orientation, thereby favoring non-productive VH-VH or VL-VL interactions during dimer formation. In contrast, the longer linker in anti-Rh(D)-6 scFv likely provides sufficient conformational flexibility to permit proper domain reorientation, enabling the formation of bivalent dimer assemblies while preserving correct antigen binding geometry. In contrast to dimers, both variants were predicted to form multiple closed trimeric assemblies spanning completely non-functional, partially functional, and fully functional configurations. In trimers, the presence of an additional scFv unit increases the number of possible domain-domain interactions, thereby enhancing the probability of correct VH-VL pairing and resulting in a broader spectrum of functional states.

The induction rate has a pronounced effect on the oligomeric distribution of both anti-Rh(D)-4 and anti-Rh(D)-6 scFvs. For both variants, fast induction conditions favor the accumulation of dimeric and

trimeric species, whereas slow induction promotes the formation of monomeric scFvs. This trend likely reflects differences in intracellular scFv concentration during expression: rapid induction leads to higher local concentrations of folding intermediates, thereby increasing the probability of intermolecular domain swapping and multimer assembly. In contrast, slower induction reduces the effective concentration of scFv chains in the periplasm, allowing intramolecular folding to predominate and favoring monomer formation.

Although the overall influence of induction rate on multimer distribution was comparable for both scFv variants, functional efficiency varied notably between multimeric subtypes, particularly between T-trimers and M-trimers. In general, functional multimer levels do not directly correlate with total multimer formation. For both scFvs, trimeric species are less functional than monomers, and higher functional trimer levels were observed under slow induction conditions, suggesting that slow induction allows sufficient time for proper domain rearrangement and correct VH-VL pairing. In contrast, rapid accumulation of scFv units under fast induction promotes non-optimized assembly of trimers, often resulting in incorrect domain swapping and mispaired VH-VL interfaces.

The distribution of trimer subtypes is influenced by linker length: in anti-Rh(D)-4, the shorter linker favors M-trimer formation, whereas in anti-Rh(D)-6, the longer linker likely facilitates proper domain orientation and correct domain swapping, resulting in a higher proportion of T-trimers.

A clear difference between the two variants is observed in dimer functionality. Anti-Rh(D)-4 scFv dimers are completely non-functional under all induction conditions, consistent with structural modeling predictions. The short linker in this variant likely restricts domain flexibility during domain swapping, favoring incorrect VH-VH or VL-VL pairing and preventing formation of a functional antigen binding interface. Similar behavior has been reported previously for anti-A scFv constructs with short linker [14]. The absence of a dimer-antigen complex in SEC analysis (Fig. 6A) further corroborates this interpretation, indicating that the anti-Rh(D)-4 dimer is unable to establish stable antigen engagement under the tested conditions.

In contrast, anti-Rh(D)-6 scFv forms functional dimers, particularly under slow induction conditions. The longer linker provides the conformational freedom required for the VH domain to reorient and correctly pair with the VL domain, enabling formation of functional antigen binding interfaces. Consistently, the detection of a dimer-antigen complex in SEC experiments (Fig. 6C) supports the conclusion that the anti-Rh(D)-6 dimer retains antigen binding competence, in agreement with the structural and functional analyses.

The dissociation constant (K_D) analysis was performed to evaluate and compare the binding parameters of monomeric and multimeric anti-Rh(D) scFv variants. Comparable K_D and B_{max} values observed for the monomer and M-trimer of anti-Rh(D)-4 scFv, as well as for the monomer and dimer of anti-Rh(D)-6 scFv, indicate that these formats predominantly exhibit monovalent binding behavior. The monovalent nature of the anti-Rh(D)-4 M-trimer can be explained by improper interaction of one scFv unit, which led to

incorrect pairing of VH and VL domains in two of the three scFv units (further explained in Supplementary Figure S6). This mispairing likely results in only a single functional antigen binding site. Similarly, the monovalent behavior of the anti-Rh(D)-6 dimer may be due to steric obstruction of the second binding site, where structural modeling shows one site exposed and oriented outward while the other faces inward and is inaccessible for antigen binding. This observation is consistent with the docking results (Fig. 4D), which demonstrated successful complex formation for only one domain within the dimeric anti-Rh(D)-6 construct, while the second domain remained sterically blocked. Consequently, despite its dimeric structure, only one binding site appears to contribute effectively to antigen interaction. This interpretation is further supported by SEC analysis, in which the anti-Rh(D)-6 dimer formed a single predominant dimer-antigen peak with an apparent molecular weight (~ 95 kDa) corresponding to one dimer (~ 50 kDa) bound to a single antigen (~ 45 kDa). The observed complex size, together with the absence of higher-molecular-weight species, supports the presence of a monovalent antigen-engaged dimer configuration.

In contrast, the trimeric forms of both anti-Rh(D)-4 and anti-Rh(D)-6 scFvs exhibited reduced binding parameters, consistent with multivalent antigen engagement in which multiple binding sites within a single trimer simultaneously interact with antigen molecules. These results differ from MMPBSA analysis, where similar binding free energies were observed across monomeric, B-dimer, and T-trimer constructs, indicating the absence of cooperative binding effects among multimerized scFv domains. The discrepancy between ELISA and MMPBSA results is expected, as MMPBSA estimates intrinsic molecular interaction energy under idealized conditions, whereas ELISA reflects apparent binding behavior influenced by avidity effects, antigen immobilization, and steric factors.

The ability of multimeric anti-Rh(D) scFvs to mediate hemagglutination was evaluated using standard and potentiator-enhanced (PEH) assays. Because these multimers are smaller than IgG antibodies [29], it was expected that they cannot directly crosslink RBCs under standard conditions, limiting unwanted hemagglutination. Hemagglutination depends on size and binding site accessibility (Fig. 3), and all tested multimers have exposed binding sites. The T-trimeric anti-Rh(D)-4 scFv failed to hemagglutinate RBCs due to its small size, while the dimeric anti-Rh(D)-6 scFv failed because of its monovalent nature. In contrast, the T-trimer of anti-Rh(D)-6 scFv induced mixed-field hemagglutination only under potentiator-enhanced conditions, reflecting its larger size compared to the T-trimeric form of anti-Rh(D)-4 scFv.

From an application perspective, the inability of these multimers to induce hemagglutination under standard assay conditions represents a significant advantage. Their small size and limited capacity to crosslink RBCs suggest that they could serve as effective blocking fragments without the risk of causing hemagglutination, similar to what has been demonstrated with monomeric anti-A scFv and trispecific triabody [14, 28]. This property makes them promising candidates for blocking antigen-Rh(D) on RBC surfaces, potentially facilitating the generation of universal RBCs for transfusion while minimizing hemagglutination-related complications.

Collectively, these findings demonstrate that GS linker length and induction rate critically influence the structural assembly and functional behavior of domain-swapped anti-Rh(D) scFv multimers. Longer linkers and controlled expression conditions facilitate proper VH-VL pairing, enabling the formation of structurally defined and functionally competent higher-order multimers.

Despite providing experimental validation of scFv multimer formation and function, this study has several limitations. First, structural interpretation of multimer formation was primarily based on computational modeling and MD simulations, which may not fully represent the exact three-dimensional folding and dynamic behavior of the proteins. Direct experimental structural determination using techniques such as X-ray crystallography (XRC) or nuclear magnetic resonance (NMR) spectroscopy could be employed in future studies to validate domain orientation and multimer architecture. Second, binding parameters were determined using ELISA-based equilibrium assays, which provide limited kinetic information on antigen–antibody interactions. Alternative methods such as surface plasmon resonance (SPR), bio-layer interferometry (BLI), or isothermal titration calorimetry (ITC) can be utilized in future work to obtain more precise kinetic and thermodynamic binding profiles. Third, long-term stability, aggregation propensity, and thermal resilience of the purified multimers were not extensively evaluated. Future studies should focus on comprehensive biophysical characterization, high-resolution structural validation, and advanced kinetic binding analyses to further optimize scFv multimer design and functional performance.

Conclusion

This study demonstrated that GS linker length and expression induction rate strongly influence the structural assembly and functional behavior of domain-swapped anti-Rh(D) scFv multimers expressed in *E. coli* Lemo21(DE3). Longer linkers facilitated correct VH-VL domain pairing and enabled the formation of functional higher-order multimers, particularly trimers and dimers in the anti-Rh(D)-6 variant. Computational modeling, docking, and functional assays confirmed that proper domain orientation is essential for maintaining antigen binding competence. These findings provide valuable insights into the design and expression of functional scFv multimers, highlighting strategies to optimize multimer formation while preserving binding activity for therapeutic and diagnostic applications. Importantly, the demonstrated lack of hemagglutination under standard conditions further supports their potential use as safe antigen-blocking agents, particularly for antigen-Rh(D) blocking to generate universal RBCs for transfusion purposes.

Declarations

Ethics approval

The study was conducted in accordance with the principles of the Declaration of Helsinki and was approved by the Institutional Review Board (IRB) of the National University of Sciences and Technology (NUST) (IRB reference number: 09-2023-ASAB-01/02). All procedures were performed in accordance

with relevant institutional and regulatory guidelines. Written informed consent to participate was obtained from all participants prior to the collection of blood samples.

Consent for publication

Not applicable.

Availability of data and materials

All data generated or analyzed during this study are included in this published article and its supplementary information files.

Competing interests

The authors declare that they have no conflicts of interest.

Funding

This research was supported by a PhD student's research funds from the Atta-Ur-Rahman School of Applied Biosciences (ASAB) at the National University of Sciences and Technology (NUST) in Sector H-12, Islamabad, Pakistan. Muhammad Asghar was supported by Ragnar Söderberg Foundation Sweden (M13/18).

Authors' contributions

SH and MA conceptualized and designed the study. SH developed the methodology and performed the software analysis. Validation was carried out by SH and MA. Formal analysis and investigation were performed by SH. Resources were provided by MA. The original draft of the manuscript was prepared by SH, and both SH and MA contributed to reviewing and editing the manuscript. Visualization was performed by SH and MA. Supervision of the study was provided by MA. All authors have read and approved the final manuscript.

References

1. de Aguiar RB, da Silva T, Costa BA, et al. Generation and functional characterization of a single-chain variable fragment (scFv) of the anti-FGF2 3F12E7 monoclonal antibody. Sci Rep. 2021;11:1432.
2. Hudson PJ, Kortt AA. High avidity scfv multimers; diabodies and triabodies. J Immunol Methods. 1999;231(1–2):177–89.
3. Zhao J, Yang L, Gu Z, et al. Stabilization of the single-chain fragment variable by an interdomain disulfide bond and its effect on antibody affinity. Int J Mol Sci. 2010;12(1):1–11.
4. Gaciarz A, Veijola J, Uchida Y, et al. Systematic screening of soluble expression of antibody fragments in the cytoplasm of E. coli. Microb Cell Fact. 2016;15:22.

5. Ahmad ZA, Yeap SK, Ali AM, Ho WY, Alitheen NB, Hamid M. scFv antibody: principles and clinical application. Clin Dev Immunol. 2012;2012:1–15.
6. Koti M, Nagy E, Kaushik AK. A single point mutation in Framework Region 3 of heavy chain affects viral neutralization dynamics of single-chain FV against bovine herpes virus type 1. Vaccine. 2011;29(41):7905–12.
7. Marcotte H, Hammarström L. Passive Immunization: Toward Magic Bullets. In: Mestecky J, editor. Mucosal Immunol. 4th ed. Academic; 2015. pp. 1403–34.
8. Le Gall F, Kipriyanov SM, Moldenhauer G, Little M. Di-, tri- and tetrameric single chain FV antibody fragments against human CD19: effect of valency on cell binding. FEBS Lett. 1999;453(2):164–8.
9. Bates A, Power CA. David vs. Goliath: the structure, function, and clinical prospects of antibody fragments. Antibodies. 2019;8(3):28.
10. Dolezal O, Pearce LA, Lawrence LJ, McCoy AJ, Hudson PJ, Kortt AA. scFv multimers of the anti-neuraminidase antibody NC10: shortening of the linker in single-chain FV fragment assembled in VL to VH orientation drives the formation of dimers, trimers, tetramers and higher molecular mass multimers. Protein Eng Des Sel. 2000;13(9):565–74.
11. Fernández LA. Prokaryotic expression of antibodies and affibodies. COBIOT. 2004;15:364–73.
12. Jugniot N, Bam R, Paulmurugan R. Expression and purification of a native thy1-single-chain variable fragment for use in molecular imaging. Sci Rep. 2021;11:23026.
13. Kalinovsky DV, Kholodenko IV, Kibardin AV, et al. Minibody-based and scfv-based antibody fragment-drug conjugates selectively eliminate GD2-positive tumor cells. Int J Mol Sci. 2023;24(3):1239.
14. Hafeez S, Zaidi NUSS. Prevention of blood incompatibility related hemagglutination: blocking of antigen A on red blood cells using in silico designed recombinant anti-A scFv. Antibodies (Basel). 2024;13(3):64. 10.3390/antib13030064.
15. Siegel DL, Chang TY, Russell SL, Bunya VY. Isolation of cell surface-specific human monoclonal antibodies using phage display and magnetically-activated cell sorting: applications in immunohematology. J Immunol Methods. 1997;205(2):169–81. 10.1016/S0022-1759(97)00087-2.
16. Yang J, Yan R, Roy A, et al. The I-TASSER suite: protein structure and function prediction. Nat Methods. 2015;12(1):7–8.
17. Chen S, Bharadwaj V, Christoffer C, et al. LZerD webserver for pairwise and multiple protein docking. Nucleic Acids Res. 2021;49(W1):W359–65.
18. Schrödinger LLC. The PyMOL molecular graphics system, version 3.1. 2025. Available from: https://pymol.org/
19. National Center for Biotechnology Information. Rh blood group D antigen [Homo sapiens] (Accession No. QYS16062.1). GenBank. Available from: https://www.ncbi.nlm.nih.gov/protein/QYS16062.1
20. Abraham MJ, Murtola T, Schulz R, et al. GROMACS: high performance molecular simulations through multi-level parallelism from laptops to supercomputers. SoftwareX. 2015;1–2:19–25.

21. Brahma R, Raghuraman H. Cost-effective purification of membrane proteins using a dual-detergent strategy. Curr Protoc Protein Sci. 2022;2(6):e452. 10.1002/cpz1.452.
22. Gasteiger E, Hoogland C, Gattiker A, et al. Protein identification and analysis tools on the ExPASy server. In: Walker JM, editor. Proteomics Protocols Handb. Humana; 2005. pp. 571–607. 10.1385/1-59259-890-0:571.
23. GraphPad Software. Nonlinear regression curve fitting was performed using GraphPad Prism version 9.5.1. 2023. Available from: https://www.graphpad.com/
24. Bruce B. Enzyme treatment of red blood cells: use of ficin and papain. Immunohematology. 2022;38(3):90–5. 10.21307/immunohematology-2022-048.
25. Fernandes HP, Cesar CL, Barjas-Castro ML. Electrical properties of the red blood cell membrane and immunohematological investigation. Rev Bras Hematol Hemoter. 2011;33(4):297–301. 10.5581/1516-8484.20110080.
26. Nance SJ, Garratty G. Polyethylene glycol: a new potentiator of red blood cell antigen–antibody reactions. Am J Clin Pathol. 1987;87(5):633–5. 10.1093/ajcp/87.5.633.
27. Woiszwillo JE. TMB formulation for soluble and precipitable HRP-ELISA. US Patent. 1991;5:006461.
28. Hafeez S, Asghar M. Enhancing red blood cell compatibility: in vitro hemagglutination prevention using a trispecific triabody as a blocking fragment for blood group antigens. J Biol Eng. 2026. 10.1186/s13036-026-00661-w.
29. Harris LJ, Skaletsky E, McPherson A. Crystallographic structure of an intact IgG1 monoclonal antibody. J Mol Biol. 1998;278(2):269–91. 10.1006/jmbi.1997.1508.

Figures

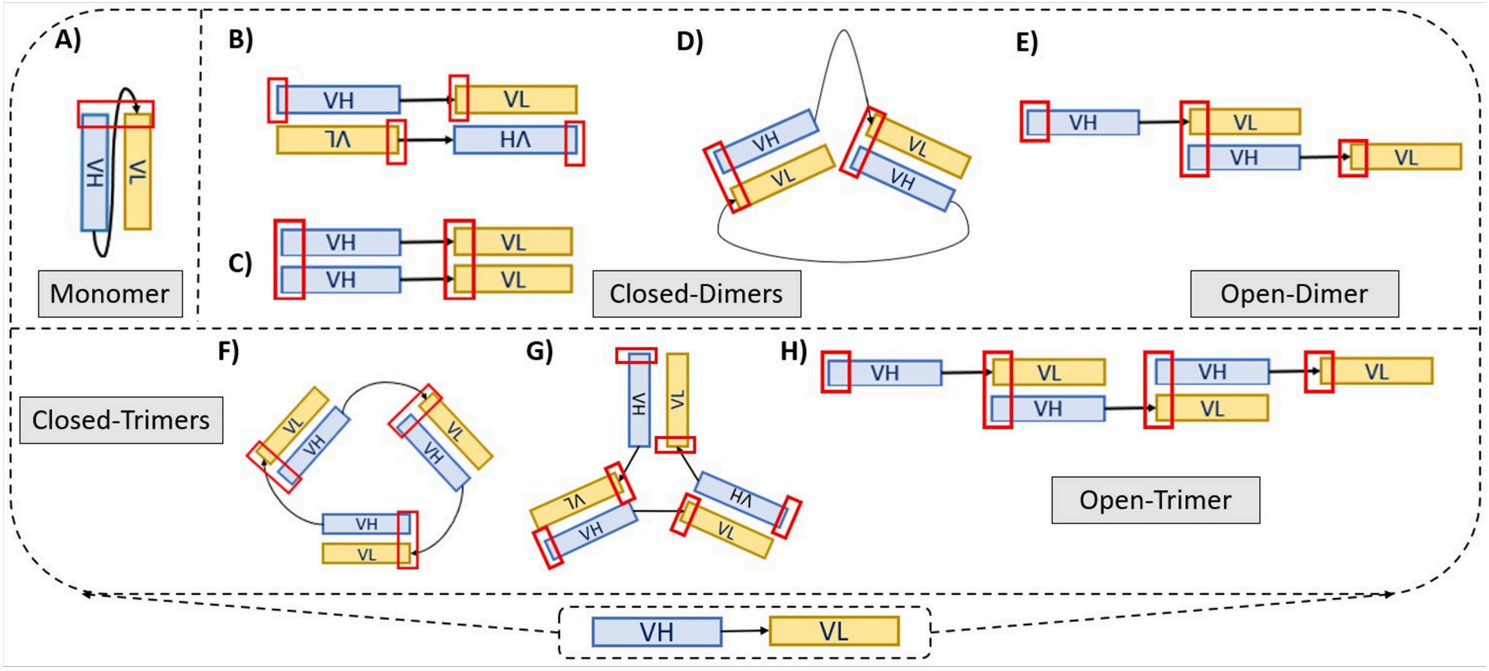


Figure 1

Schematic diagrams of all theoretically possible multimeric $(scFv)_x$ structures derived from anti-Rh(D)-4 and anti-Rh(D)-6 scFv sequences. A) Closed functional monomeric anti-Rh(D) scFv, B and C) closed non-functional dimers, D) closed functional (bivalent) dimer, E) open half functional (monovalent) dimer, F) closed functional (trivalent) trimer, G) closed non-functional trimer and H) open half functional (bivalent) trimer. Red boxes show binding sites. Black arrow represents GS linker.

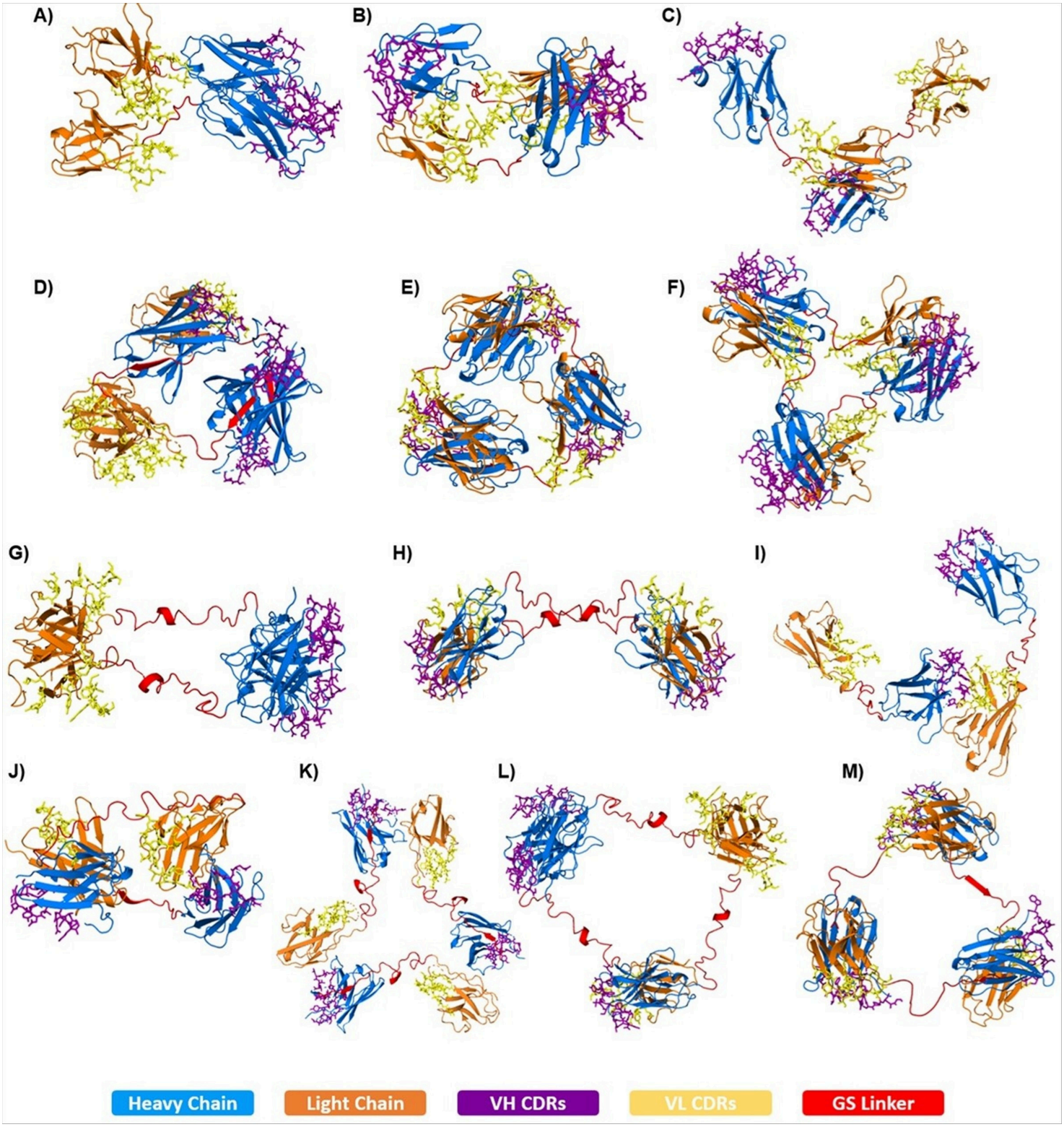


Figure 2

Models of multimer $(scFv)_x$ made from the open chains of anti-Rh(D) scFvs variants. A-F) Models generated by open chains of anti-Rh(D)-4 scFv. A and B) Non-functional dimers-A4 and B4, C) monovalent dimer-C4, D) monovalent trimer-A4 and E) trivalent trimer-B4, F) non-functional trimer-C4. G and M) Models generated by open chains of anti-Rh(D)-6 scFv. G and H) Non-functional dimers-A6 and B6, I) monovalent dimer-C6, J) bivalent dimer-D6 K) non-functional trimer-A6, L) monovalent trimer-B6 and M) trivalent trimer-C6.

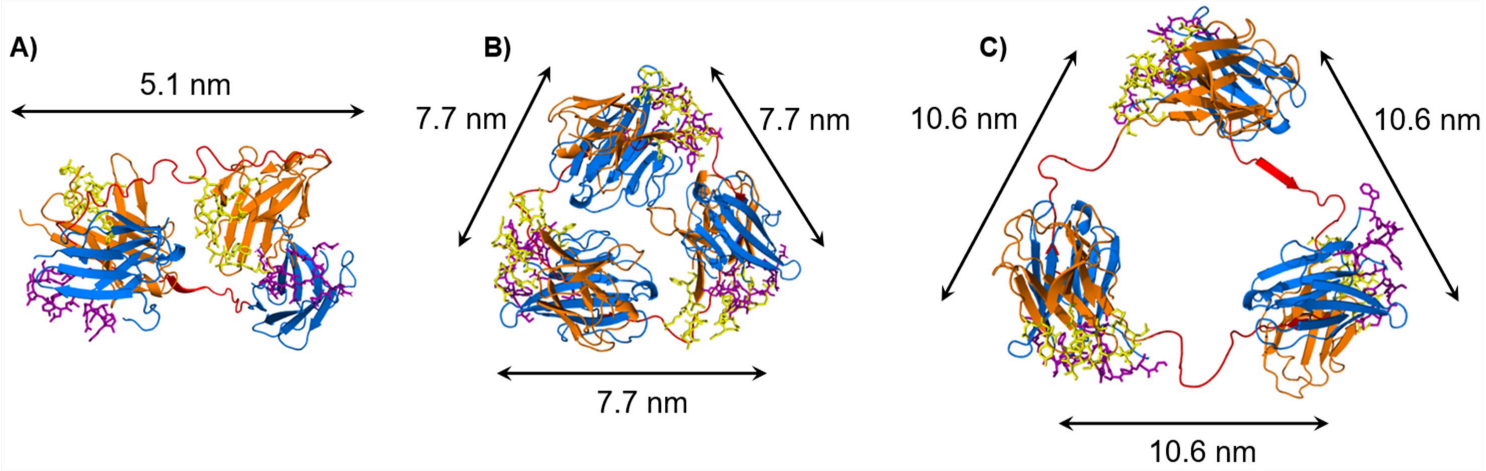


Figure 3

Molecular dimensions of A) dimer-D6, B) trimer-B4 and C) trimer-C6

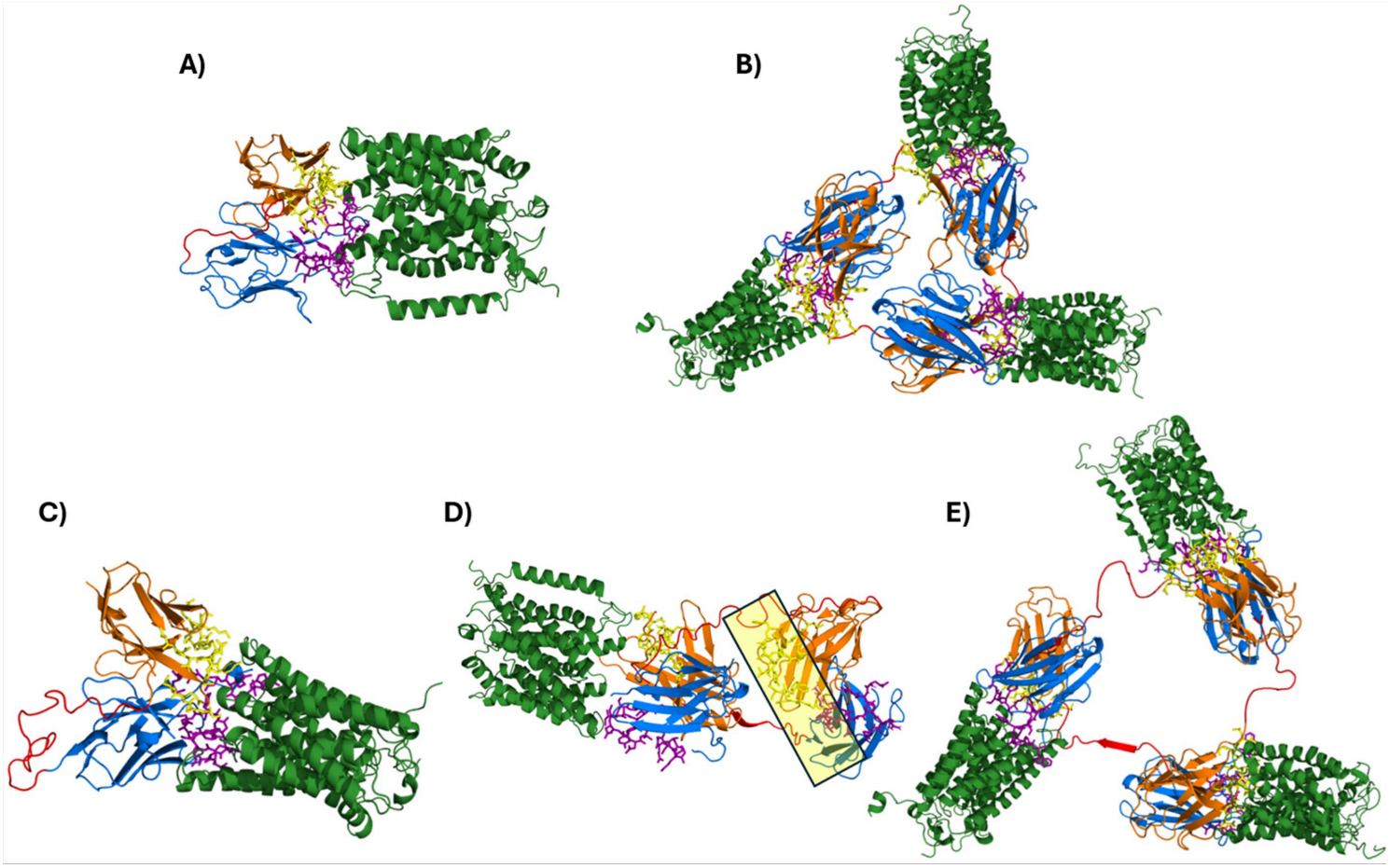


Figure 4

Docked poses of anti-Rh(D) scFv constructs with antigen-Rh(D). A) Complex of monomeric anti-Rh(D)-4 scFv with antigen-Rh(D). B) Trimeric anti-Rh(D)-4 scFv bound to three antigen-Rh(D) molecules. C) Complex of monomeric anti-Rh(D)-6 scFv with antigen-Rh(D). D) Dimeric anti-Rh(D)-6 scFv showing only one accessible antigen binding site. The yellow box represents the sterically blocked binding site. E) Trimeric anti-Rh(D)-6 scFv simultaneously bound to three antigen-Rh(D) molecules. Antigen-Rh(D) is shown in green.

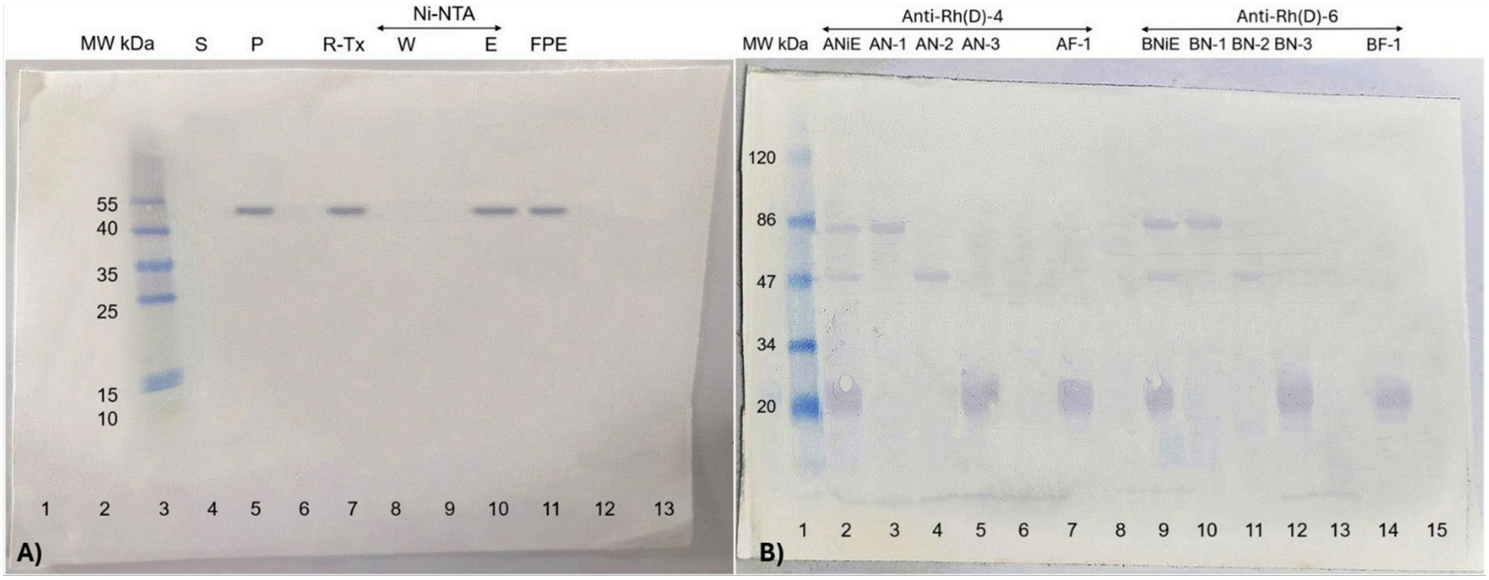


Figure 5

Western blot analysis of the purification of the A) transmembrane antigen Rh(D) and B) variants of anti-Rh(D) scFv. A) Lanes 4 and 5 show the crude lysate fractions: supernatant (S) and pellet (P), respectively, with the pellet containing the recombinant antigen-Rh(D) band at ~45 kDa.

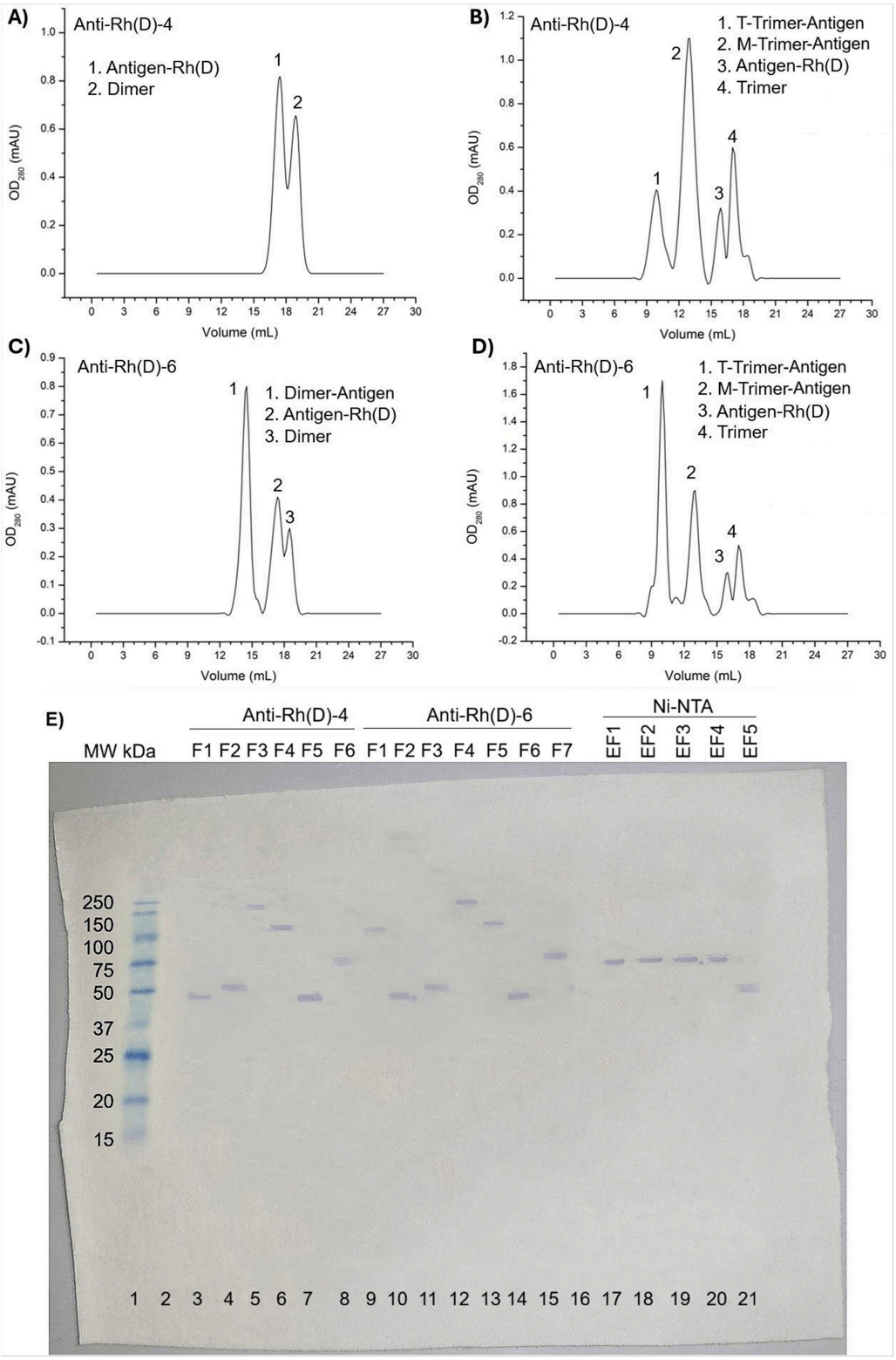


Figure 6

SEC profiles and western blot analysis of anti-Rh(D) scFv variants. SEC profiles of A) dimeric and B) trimeric anti-Rh(D)-4 scFv in complex with antigen-Rh(D). SEC profile of C) dimeric and D) trimeric anti-Rh(D)-6 scFv in complex with antigen-Rh(D). Chromatograms were monitored at 280 nm (OD_{280}) as a function of elution volume (mL). E) Western blot analysis of selected SEC and Ni-NTA purified fractions. Lanes 3-8 show SEC-purified fractions of anti-Rh(D)-4 scFv corresponding to antigen (~45 kDa), dimer

(~50 kDa), T-trimer-antigen (~210 kDa), M-trimer-antigen (~120 kDa), unbound antigen-Rh(D) (~45 kDa), and unbound trimer (~75 kDa). Lanes 9-11 show SEC-purified fractions of anti-Rh(D)-6 scFv representing dimer-antigen (~95 kDa), unbound antigen-Rh(D) (~45 kDa), and unbound dimer (~50 kDa). Lanes 12-15 show T-trimer-antigen (~210 kDa), M-trimer-antigen (~120 kDa), unbound antigen-Rh(D) (~45 kDa), unbound trimer (~75 kDa), Lanes 17 and 18 show Ni-NTA-purified T-trimer and M-trimer (~75 kDa) of anti-Rh(D)-4, while lanes 19-21 show Ni-NTA-purified T-trimer, M-trimer (~75 kDa), and dimer (~50 kDa) of anti-Rh(D)-6.

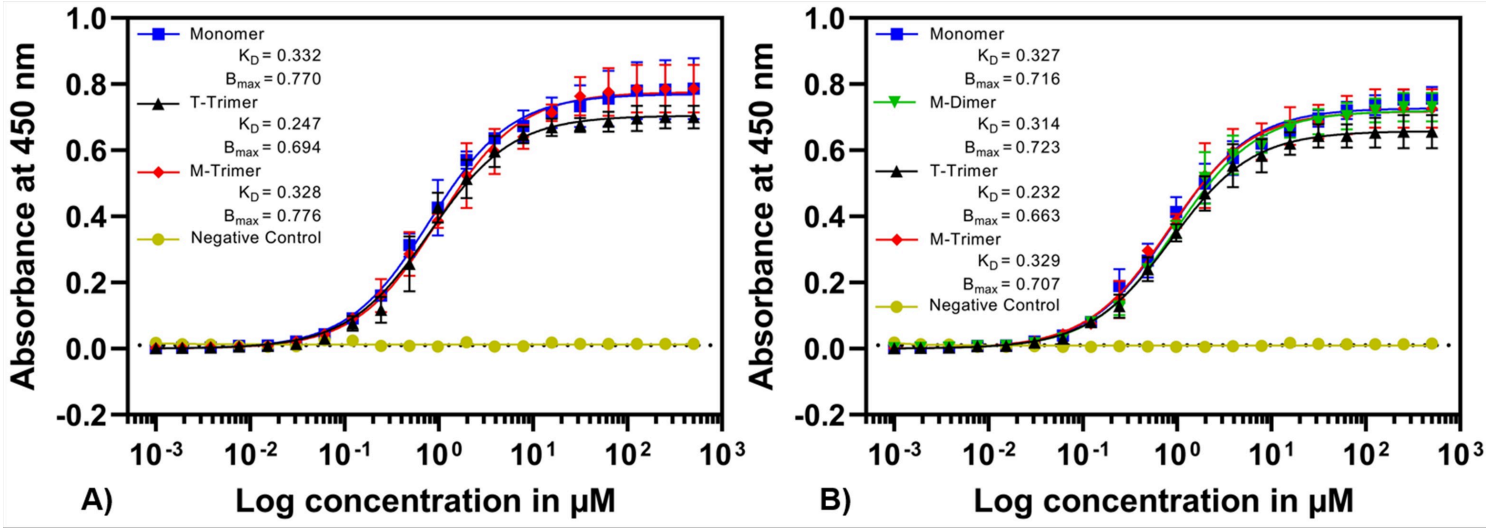


Figure 7

Binding parameters of A) anti-Rh(D)-4 scFv and B) anti-Rh(D)-6 scFv.

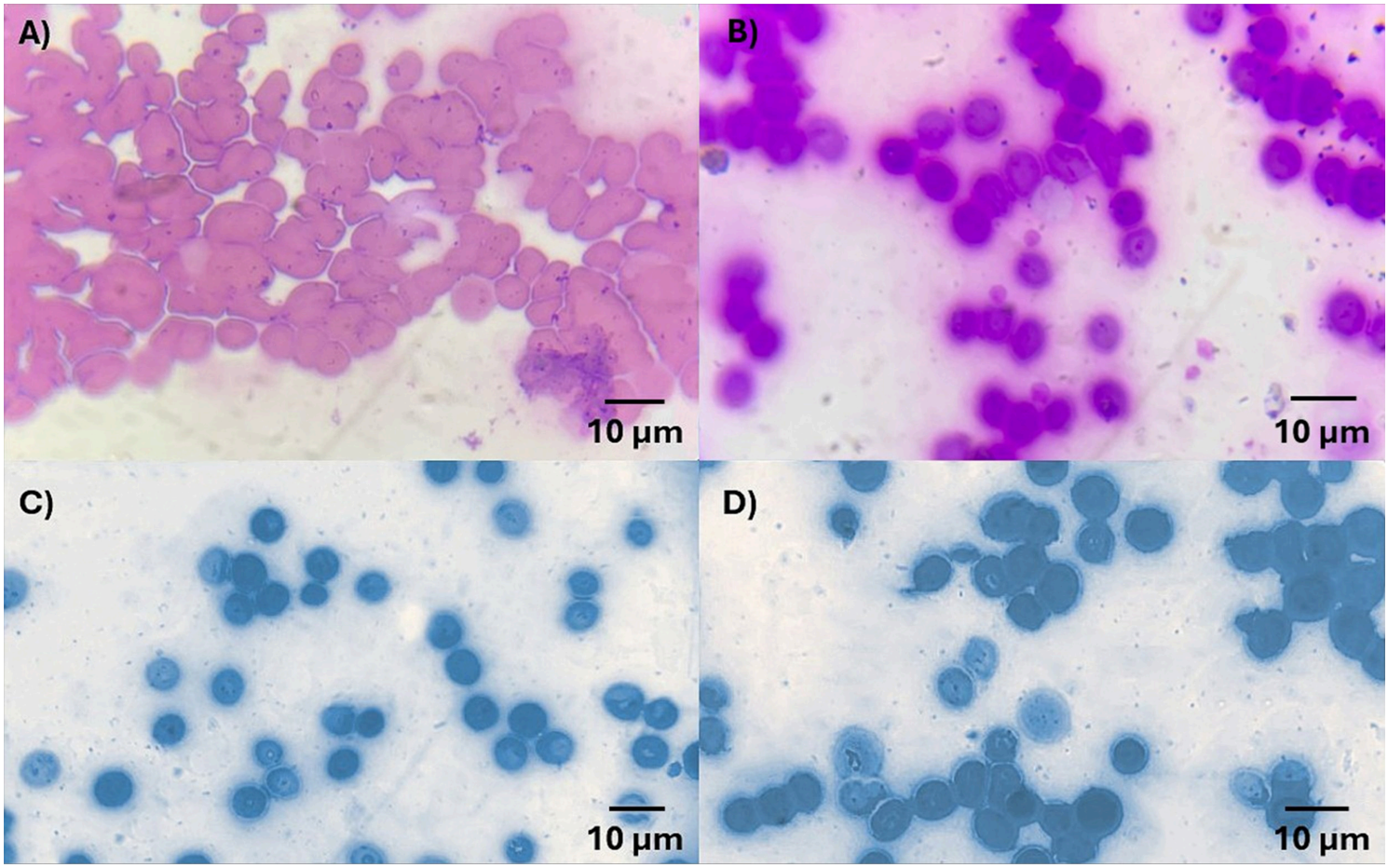


Figure 8

Microscopy images of O+ RBCs coated with or without multimers of anti-Rh(D)-4 scFv: A) IgM-mediated hemagglutination (control), (B) uncoated, non-hemagglutinated cells under potentiator-enhanced conditions (control), (C) T-trimer coated, non-hemagglutinated (standard conditions) and (D) T-trimer coated, non-hemagglutinated (potentiator-enhanced conditions).

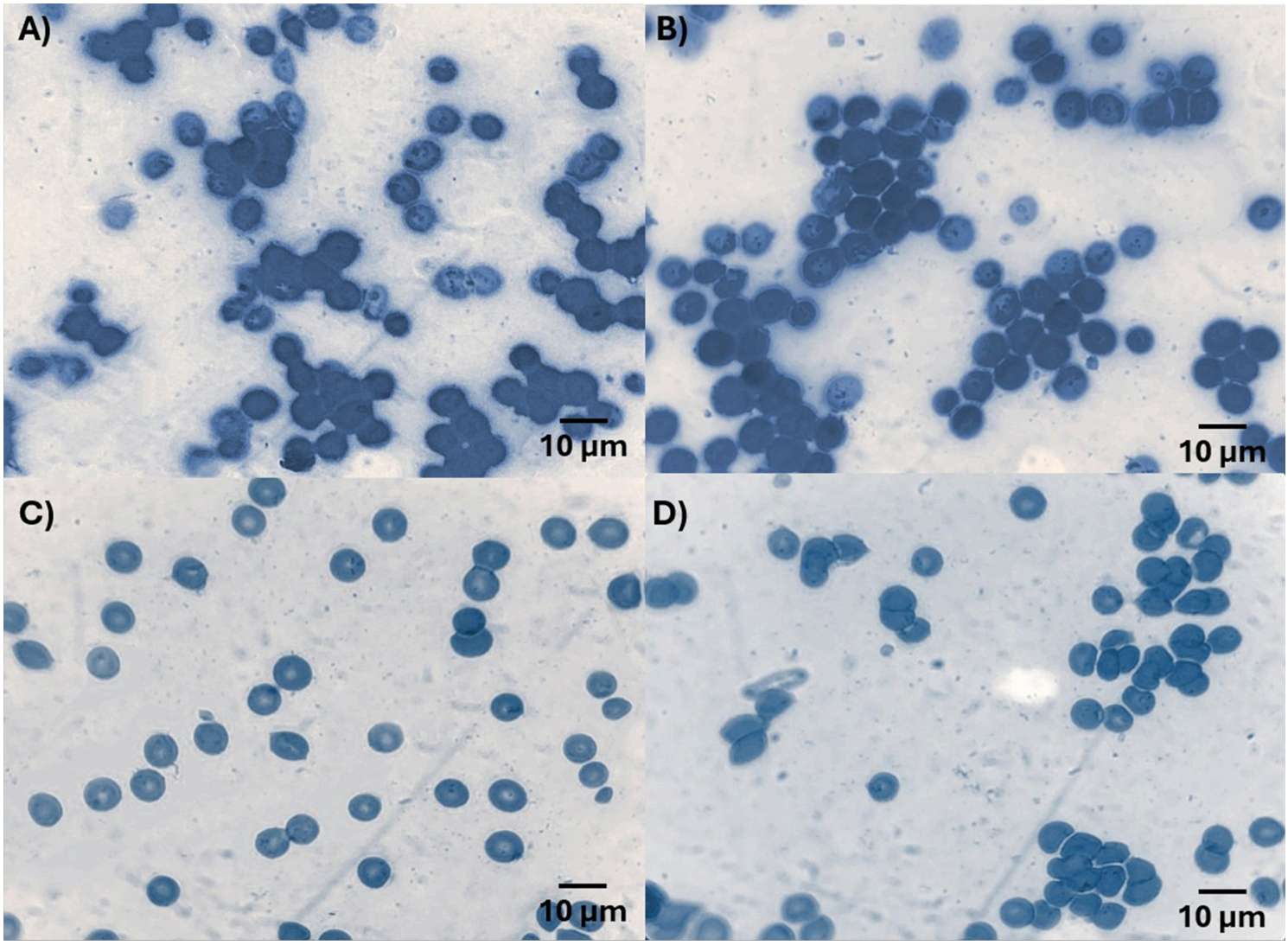


Figure 9

Microscopy images of O+ RBCs coated with multimers of anti-Rh(D)-6 scFv: A) dimer coated, non-hemagglutinated (standard conditions); (B) dimer coated, non-hemagglutinated (potentiator-enhanced); (C) T-trimer coated, non-hemagglutinated (standard conditions); (D) T-trimer coated, mixed-field hemagglutination (potentiator-enhanced).

Supplementary Files

This is a list of supplementary files associated with this preprint. Click to download.

- AntiRhSupplementary.docx